Stem Cell Reports
Article

ISSCR

OPEN ACCESS

Developmental Potential and Plasticity of Olfactory Epithelium Stem Cells Revealed by Heterotopic Grafting in the Adult Brain

Qian Li,[1] Tiziano Siri,[1] Cedric Bressan,[1] Yves de Koninck,[1,2] and Armen Saghatelyan[1,2,*]
[1]CERVO Brain Research Center, Quebec City, QC G1J 2G3, Canada
[2]Department of Psychiatry and Neuroscience, Université Laval, Quebec City, QC G1K 7P4, Canada
*Correspondence: armen.saghatelyan@fmed.ulaval.ca
https://doi.org/10.1016/j.stemcr.2020.03.008

SUMMARY

The neural stem cells (NSCs) residing in the olfactory epithelium (OE) regenerate damaged olfactory sensory neurons throughout adulthood. The accessibility and availability of these NSCs in living individuals, including humans, makes them a promising candidate for harvesting their potential for cell replacement therapies. However, this requires an in-depth understanding of their developmental potential after grafting. Here, we investigated the developmental potential and plasticity of mouse OE-derived NSCs after grafting into the adult subventricular zone (SVZ) neurogenic niche. Our results showed that OE-derived NSCs integrate and proliferate just like endogenous SVZ stem cells, migrate with similar dynamics as endogenous neuroblasts toward the olfactory bulb, and mature and acquire similar electrophysiological properties as endogenous adult-born bulbar interneurons. These results reveal the developmental potential and plasticity of OE-derived NSCs *in vivo* and show that they can respond to heterotopic neurogenic cues to adapt their phenotype and become functional neurons in ectopic brain regions.

INTRODUCTION

Neural stem cells (NSCs) in the olfactory epithelium (OE) replenish the population of sensory neurons throughout life and retain a lifelong capacity of regeneration upon injury (Brann et al., 2015; Mackay-Sim and Kittel, 1991). Newly generated sensory neurons project their axons to the olfactory bulb (OB) where they establish axo-dendritic synapses with the primary dendrites of mitral and tufted cells, the principal bulbar neurons (Nagayama et al., 2014). As OE is a nerve tissue exposed to the external environment, it can be biopsied to isolate and culture NSCs without altering sensory processing (Andrews et al., 2016; Girard et al., 2011). Olfactory stem cells have been used for investigating the pathological features of neurodevelopmental and neurodegenerative disorders, such as autism spectrum disorder (Feron et al., 2016; Nguyen et al., 2016), schizophrenia (Lavoie et al., 2017), bipolar disorder (Schroeder et al., 2016), Alzheimer (Ayala-Grosso et al., 2015), and Parkinson (Cook et al., 2011) diseases. Given the accessibility and availability of large quantities of NSCs, they also show great promise for cell replacement therapies. It should be mentioned that, unlike induced pluripotent stem cells (iPSCs), these NSCs do not require genetic modifications for neuronal lineage conversion. It has previously been shown that OE-derived NSCs possess developmental potency that can be directed toward the generation of cell types in host tissues after grafting (Murrell et al., 2005). Since then, a number of studies have shown that OE-derived stem cells are able to self-renew *in vitro* and possess repair potential in models of stroke (Fan et al., 2018), Parkinson disease (Abdel-Rahman et al., 2018), and hearing loss (Xu et al., 2016). Although these studies showed that OE-derived NSCs have a potential for use in autologous stem cell therapies for brain disorders, their full developmental profile and plasticity are unknown. Can they differentiate into completely distinct neuronal phenotypes in response to different micro-environmental cues and, if so, can they acquire morpho-functional properties similar to those of endogenous neurons in ectopic brain regions.

Interestingly, the adult brain harbors another neurogenic region in the subventricular zone (SVZ) where NSCs lining the lateral ventricle walls give rise to immature neurons known as neuroblasts (Alvarez-Buylla and García-Verdugo, 2002; Gengatharan et al., 2016). These neuroblasts first migrate tangentially through the rostral migratory stream (RMS) and then radially, in different OB layers where they mature and become functional bulbar interneurons (Gengatharan et al., 2016). Adult-born OB interneurons are axonless cells and form dendro-dendritic reciprocal synapses with principal neurons (Lledo and Saghatelyan, 2005; Whitman and Greer, 2007). They are involved in odor processing, and altering their number and/or function affects several types of olfactory behavior, including fine odor discrimination, short-term odor memory, and olfactory learning (Alonso et al., 2012; Breton-Provencher et al., 2009; Grelat et al., 2018; Hardy et al., 2018; Malvaut et al., 2017). Thus, NSCs in the OE and SVZ are exposed to completely different micro-environmental cues, undergo different developmental trajectories, and generate completely different neuronal subtypes with distinct morpho-functional characteristics.

Previous studies have shown that stem cells isolated from one region, when transplanted into another region, integrate the host micro-environment and generate neurons and glia that resemble ectopic region-specific cell types (Seidenfaden et al., 2006; Shihabuddin et al., 2000; Suhonen et al., 1996). These studies were mostly based on the phenotypic characterization of grafted cells by determining the expression of cell-type-specific markers and general morphological appearance. However, it is not known whether the morpho-functional properties of grafted and endogenous cells are similar or whether the differentiation of grafted NSCs into region-specific cells follows the same developmental trajectory.

In this study, we used a highly accessible source of OE-derived NSCs for cell replacement therapies to explore their developmental potential and trajectories for generating ectopic neuronal subtypes. We also performed full morpho-functional assessments of grafted and endogenous neurons. Olfactory NSCs were isolated from the OE of adult mice and were cultured as neurospheres before heterotopic engraftment in the adult mouse SVZ. We used cell-type-specific markers for the SVZ niche to show that grafted OE-derived NSCs and endogenous SVZ NSCs are indistinguishable. Like endogenous neuroblasts in the RMS, the migrating grafted cells were doublecortin (DCX) positive and glial fibrillary acidic protein (GFAP) negative, confirming their neuroblast identity. Time-lapse imaging data showed that the migrating parameters of OE NSC-derived cells are the same as those of endogenous neuroblasts in the RMS in terms of displacement distance, speed of migration, and duration of the migratory phases. The grafted cells also had similar trajectories in terms of neuronal maturation and acquired morphometric characteristics that made them indistinguishable from endogenous adult-born neurons. Importantly, OE-derived cells became functional OB neurons with passive and active membrane properties similar to those of endogenous adult-born interneurons, fully integrated the bulbar network, and received similar levels of spontaneous excitatory inputs. Our results showed that OE-derived NSCs make up a population of easily accessible and expandable cells that can respond to different micro-environmental cues and that can differentiate into neurons in an ectopic brain region with the same developmental trajectories and morpho-functional properties as endogenous NSCs.

RESULTS

Isolation of NSCs from the OE

The olfactory mucosa was dissected bilaterally from the nasal cavities of adult mice. The OE tissue containing NSCs was separated from the lamina propria, dissociated mechanically, and plated in serum-containing growth medium. They served as the primary culture. When confluency was reached, the cells were transferred to a serum-free medium for neurosphere induction. As shown in Figure 1A, cell clusters were formed while attaching to the wall of the culture flask and evolved into 3D neurospheres after detaching. Neurospheres were collected at the peak of production for the experiments described below. In parallel experiments, we have also cultured lamina propria stem cells and observed faster formation of spheres in the serum-free induction medium (Figure S1).

OE-Derived NSCs Integrate the SVZ and Proliferate such as Endogenous Stem Cells

To study the integration of OE-derived NSCs into the SVZ niche of adult mice, we immunolabeled for cell-type-specific markers 4 days after grafting of OE-derived NSCs. Free-floating neurospheres were dissociated, infected with GFP-encoding lentiviral particles, and a day later were transplanted into the ventral and dorsal sites of the SVZ. For the control group, a GFP-encoding virus was injected at the same coordinates to determine the endogenous cell populations in the SVZ infected by the same lentiviral particles. At 4 days post-injection (4 dpi), the animals were sacrificed, and sagittal brain sections were immunostained for Ki67, Nestin, DCX, and GFAP (Figure 1B). We first examined the expression of these markers *in vitro* in the OE-derived neurospheres. Although DCX was not detected in cells dissociated from free-floating OE neurospheres, Ki67 and Nestin, the proliferative and NSC markers, respectively, were expressed in 62.0% ± 3.3% (n = 130 cells from 3 biological replicates) and 41.8% ± 4.7% (n = 216 cells from 3 biological replicates) of cells. After grafting, the OE-derived NSCs had integrated the SVZ, and only 16% expressed the proliferative marker Ki67. This percentage was similar to that of endogenous SVZ proliferative cells (Figure 1C, endogenous: 15.6% ± 2.9%, n = 641 cells from 3 mice; grafted: 22.4% ± 3.8%, n = 637 cells from 3 mice). The majority of the grafted cells expressed Nestin, which was very similar to the expression pattern of endogenous cells (Figure 1C, endogenous: 65.5% ± 1.3%, n = 457 cells from 3 mice; grafted: 66.5% ± 5.3%, n = 365 cells from 3 mice). In addition, no significant differences were found between the grafted and endogenous cells in terms of the percentages of GFAP- and DCX-expressing cells (Figure 1C, for GFAP: endogenous: 11.4% ± 0.3%, n = 184 cells from 3 mice; grafted: 17.9% ± 5.2%, n = 272 cells from 3 mice; and for DCX: endogenous: 7.7% ± 3.0%, n = 641 cells from 3 mice; grafted: 10.6% ± 4.5%, n = 637 cells from 3 mice). These results suggest that the heterogeneity of the grafted cells resembles that of the

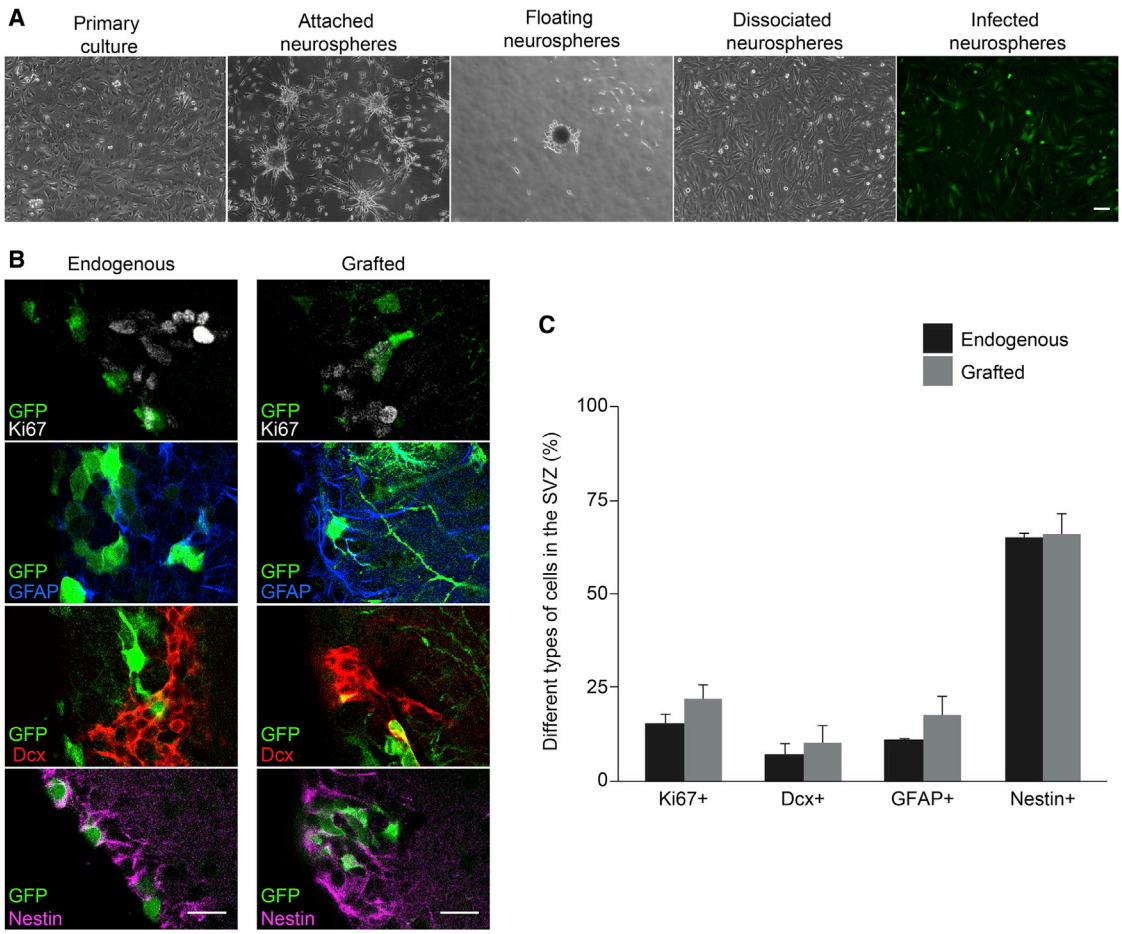

Figure 1. The Proliferation and Cell Heterogeneity of OE-Derived NSCs in the SVZ after Heterotopic Grafting

(A) OE-derived NSCs were expanded in growth medium. Neurospheres were induced, collected at the peak of production, and infected with CMV-GFP lentiviruses before grafting.

(B) Representative images of endogenous SVZ cells and grafted OE-derived NSCs used to analyze the expression of cell-type-specific markers.

(C) Quantification of endogenous and grafted cell populations in the SVZ. No significant differences were observed in the percentages of cells expressing Ki67, DCX, GFAP, or Nestin between the two groups of cells. p values were calculated using an unpaired Student's t test. The data are expressed as mean ± SEM (n = 184–641 endogenous and 272–637 grafted cells from 3 mice, representing 3 independent experiments). Scale bars, 100 μm (A) and 20 μm (B).

See also Figures S1 and S2.

endogenous cells in the SVZ and that grafted cells acquire the molecular signature of endogenous SVZ cells in response to micro-environmental signals by reducing their proliferative activity and acquiring DCX and GFAP expression.

OE-Derived Cells Migrate in the RMS in the Same Way as Endogenous Neuroblasts

We next investigated whether OE-derived NSCs generate neuronal precursors that migrate long distances along the RMS to the OB like endogenous neuroblasts. We first immunolabeled for DCX and GFAP in the RMS at 8–9 dpi of OE-derived NSC grafting in the SVZ. Nearly all the cells that migrated to the RMS were DCX^+ (97.8% ± 1.1%, n = 174 cells from 3 mice) and $GFAP^-$, showing that OE-derived NSCs produce neuroblasts (Figures 2A–2C). Approximately 10% of the migrating cells in the RMS remained proliferative $Ki67^+$ cells (13.0% ± 1.6%; n = 174 cells from 3 mice). We then performed time-lapse imaging in acute brain sections from mice harboring grafted OE-derived NSCs and virally labeled endogenous neuroblasts to analyze their migratory behaviors (Video S1). There were no differences between grafted and endogenous cells in terms of track length throughout a 1-h imaging session (endogenous:

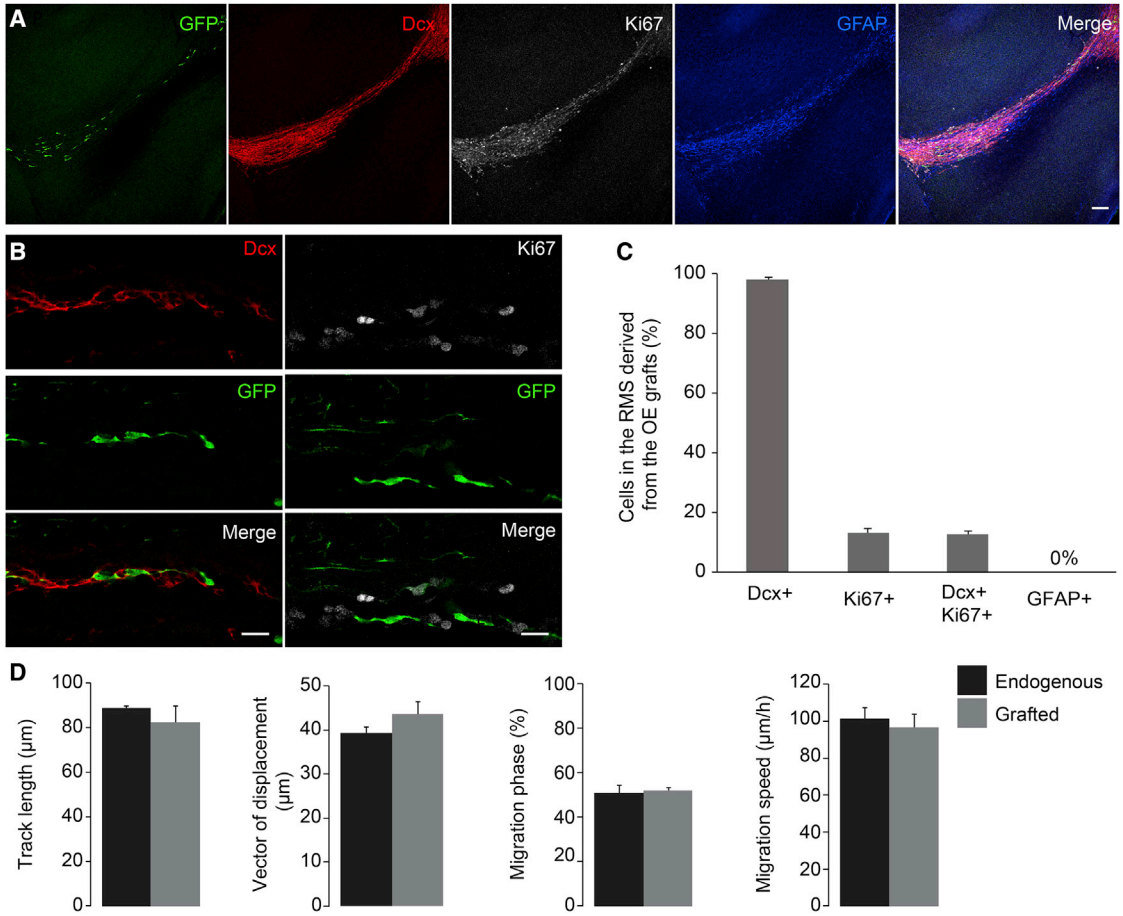

Figure 2. OE-Derived NSCs Give Rise to Migrating Neuroblasts in the RMS after Integrating the SVZ

(A–C) OE-derived NSCs were grafted into the SVZ and were detected in the RMS at 8–9 dpi (A). Migrating cells originated from the OE were identified as neuroblasts by co-labeling with DCX (B and C); n = 3 mice.

(D) The migration characteristics of the OE-derived neuroblasts were the same as those of endogenous neuroblasts in the RMS in terms of migration distance, migration vector, the percentage of migratory phases, and speed of migration; n = 75 endogenous neuroblasts and 112 grafted cells from 4 to 5 mice, respectively. The data are expressed as mean ± SEM. Scale bars, 100 μm (A) and 20 μm (B).

See also Video S1.

89.8 ± 1.1 μm, n = 75 cells from 4 mice; grafted: 82.7 ± 7.7 μm, n = 112 cells from 5 mice), the displacement vector (endogenous: 39.5 ± 1.0 μm; grafted: 43.6 ± 2.9 μm), the duration of the migratory phases (endogenous: 51.8% ± 2.6%; grafted: 52.1% ± 1.5%), or the speed of migration (endogenous: 102.9 ± 4.5 μm/h; grafted: 96.6 ± 7.4 μm/h) (Figure 2D). These results suggest that OE-derived NSCs integrate the SVZ niche and differentiate into neuronal precursors that adopt the same migratory behavior as endogenous neuroblasts.

Grafted OE-Derived NSCs Differentiate Further and Mature in the OB

To determine the differentiation and maturation of OE-derived NSCs in the ectopic brain region, we performed immunohistochemical and morphological assessments of grafted cells in the OB. Approximately 3 weeks after grafting (24 dpi) the GFP-labeled grafted neurons appeared in the bulbar network, with morphological characteristics similar to those of endogenous adult-born neurons (Figure 3A). The number of these neurons increased from 24 to 60 dpi, indicating that OE-derived NSCs in the SVZ continuously produce neuronal precursors that migrate to the OB (Figure 3A). To ascertain that these neurons are indeed originating from OE NSCs and not from lamina propria neural crest stem cells that could have been present in our OE primary culture due to the surgical separation of OE from underlying lamina propria, we also grafted GFP-labeled dissociated cells derived from lamina propria spheres into the adult SVZ. We reasoned that, if the cells

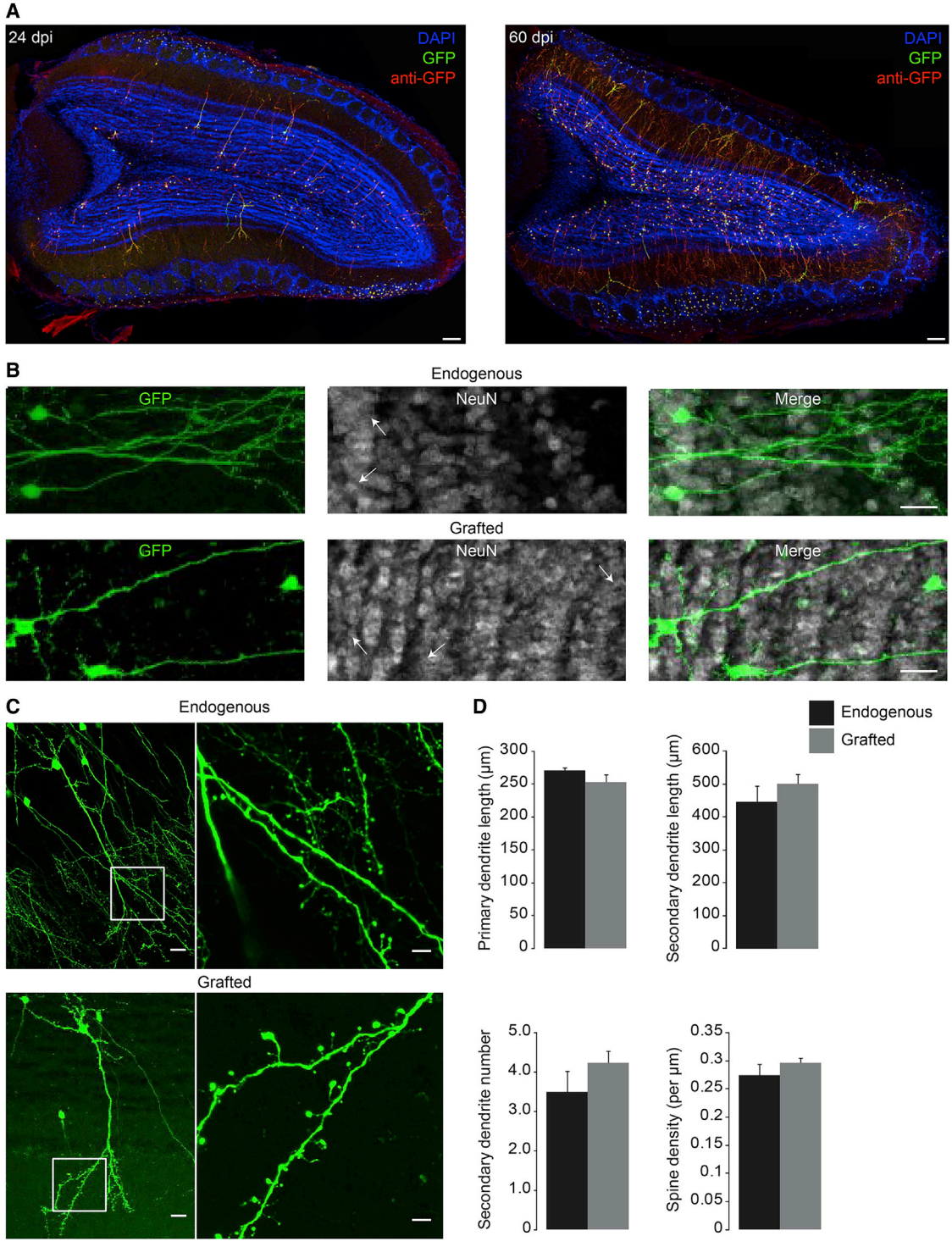

Figure 3. Cells Generated from Grafted OE-Derived NSCs Arrive and Mature in the OB

(A) OE-derived NSCs matured and evolved into mature granule cells in the OB by 24 dpi. Longer periods after grafting (60 dpi) led to a higher number of cells in the OB. OE-derived NSCs were infected with GFP-encoding lentiviruses before grafting and were immunolabeled for GFP, which produced overlapping images of virally derived GFP fluorescence (green) and GFP immunolabeling (red).

(B) Representative images of endogenous adult-born granule cells and grafted OE NSC-derived neurons in the OB immunolabeled for neuronal marker NeuN.

(legend continued on next page)

in the OB are derived from "missed" lamina propria stem cells present in the OE neurospheres preparation, then grafting of pure lamina propria stem cells should result in a higher number of grafted cells. Analysis of mice after grafting of lamina propria stem cells revealed, however, a very distinct pattern. Already at 4 dpi, GFP-labeled cells derived from lamina propria had a different appearance in the SVZ. Although grafting of OE-derived neurospheres resulted in cells leaving the graft and migrating throughout the SVZ, the cells of lamina propria remained in the graft and did not spread out in the SVZ (n = 6 hemispheres, 3 mice; Figure S2). Furthermore, no GFP-labeled lamina propria grafted cells were observed in the SVZ, RMS, or OB at 24 dpi (n = 8 hemispheres, 4 mice; Figure S2). This contrasts sharply with numerous GFP-labeled cells after the grafting of OE-derived NSCs (Figures 3 and S2) at both 4 and 24 dpi, suggesting a higher propensity for integration of grafted stem cells of neural lineage under the baseline conditions.

To determine whether cells in the OB after a grafting of OE-derived NSCs express molecular markers of mature neurons, we performed immunolabeling for neuronal markers NeuN and calretinin, which is expressed by a subpopulation of endogenous adult-born neurons (Hardy et al., 2018). The vast majority of grafted cells express the markers of mature neurons, and no differences in the expression of NeuN (endogenous: 93.4% ± 2.1%; grafted: 93.5% ± 1.2%; Figure 3B) and calretinin (endogenous: 13.3% ± 2.7%; grafted: 14.7% ± 2.4%, n = 525 and 121 cells, respectively, from 2 to 3 mice) between the grafted and endogenous neurons were observed. To characterize the morphological properties of these cells, we compared the lengths of the primary and secondary dendrites and their spine densities to those of endogenous adult-born neurons (Figure 3C). No significant morphological differences were observed between the grafted and endogenous cells in the OB in terms of primary dendrite length (endogenous: 270.8 ± 4.0 μm, n = 30 cells from 3 mice; grafted: 253.2 ± 11.4 μm, n = 30 cells from 3 mice), secondary dendrite length (endogenous: 446.7 ± 46.8 μm; grafted: 501.0 ± 29.4 μm), secondary dendrite number (endogenous: 3.5 ± 0.5; grafted: 4.2 ± 0.3), or dendritic spine density (endogenous: 0.27 ± 0.02 μm^{-1}; grafted: 0.30 ± 0.01 μm^{-1}) (Figure 3D). These results show that the grafted cells acquire the same neuronal phenotype and morphological characteristics as those of endogenous adult-born neurons.

Neurons Derived from OE NSCs Acquire Electrophysiological Properties Similar to Those of Endogenous Adult-Born OB Neurons

Although our immunohistochemical, time-lapse imaging, and morphometric analyses did not reveal any differences between endogenous neurons and those derived from OE NSCs, it remains to be determined whether grafted cells functionally integrate the OB neuronal network. We thus electrophysiologically characterized these cells and compared their properties to those of endogenous adult-born bulbar neurons. We performed patch-clamp recordings from GFP^+ grafted and endogenous cells in the OB at 28–35 dpi (Figures 4A and 4B). OE NSC-derived neurons acquired passive and active membrane properties similar to those of endogenous adult-born neurons. No differences in resting membrane potential, capacitance, or membrane resistance were observed (Table 1). OE NSC-derived neurons also acquired rapid inward and delayed outward currents typical of Na^+ and K^+ currents, respectively (Carleton et al., 2003). There were no significant differences in the activation thresholds and average Na^+ peak currents at any voltage step between the two groups of cells (Figure 4C). To determine whether grafted cells integrate the bulbar network and receive excitatory postsynaptic currents (EPSCs), we recorded spontaneous EPSC (sEPSC) and miniature EPSC (mEPSC) currents (Figure 4D). No significant differences were found in the average frequencies and amplitudes of sEPSCs and mEPSCs (sEPSCs: endogenous 0.25 ± 0.04 Hz and 5.4 ± 0.4 pA, n = 13 cells from 9 mice; grafted 0.31 ± 0.08 Hz and 4.6 ± 0.3 pA, n = 6 cells from 4 mice; mEPSCs: endogenous 0.16 ± 0.03 Hz and 5.6 ± 0.5 pA, n = 12 cells from 6 mice; grafted, 0.12 ± 0.03 Hz and 4.4 ± 0.4 pA, n = 5 cells from 3 mice; Figure 4E), or rise and decay times of mEPSCs (rise time: endogenous 4.25 ± 0.27 ms; grafted 4.36 ± 0.33 ms; decay time: endogenous 19.75 ± 1.33 ms; grafted 21.21 ± 1.73; Figure 4E) between the two groups of cells. These results show that neurons derived from OE NSCs functionally integrate the OB network and acquire electrophysiological properties similar to those of endogenous adult-born bulbar neurons.

DISCUSSION

In this study, we characterized the developmental profile and potential of OE-derived NSCs after heterotopic grafting into the adult SVZ. These two neurogenic niches contain

(C) OE-derived neurons were detected mainly in the granule cell layer of the OB and had morphological features similar to those of endogenous adult-born granule cells. The white squares indicate enlarged regions of secondary dendrites.
(D) No significant differences were observed between endogenous adult-born granule neurons and grafted cells in terms of primary dendrite length, secondary dendrite length, secondary dendrite number, or dendritic spine density (n = 30 cells from 3 mice for both groups). The data are expressed as mean ± SEM. Scale bars, 100 μm (A), 20 μm (B and C, left panels), and 5 μm (C, right panels).
See also Figure S2.

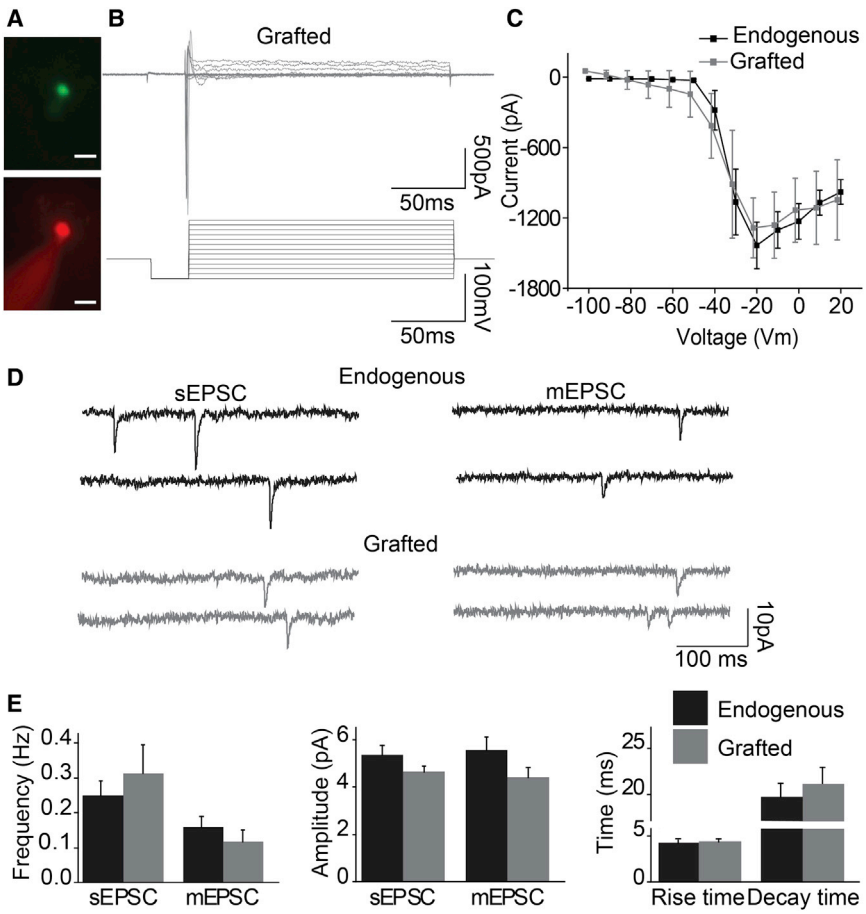

Figure 4. Mature Neurons Derived from OE NSCs Exhibit Electrophysiological Properties Similar to Those of Endogenous Adult-Born Neurons in the OB

(A) An example of a recorded OE-derived neuron, showing GFP viral labeling (green) and co-labeling with Alexa Fluor 594 (red), which was added to the intracellular patch solution.

(B) Example of membrane currents recorded from the neuron derived from OE NSCs graft induced by a range of potentials in 10-mV increments.

(C) Current-voltage curves generated during the voltage pulses. No significant differences in average current values were observed at any voltage step.

(D) Examples of sEPSCs and mEPSCs recorded from endogenous adult-born granule cells and neurons derived from OE NSCs in the OB.

(E) No significant differences were identified in average frequencies and amplitudes of sEPSCs and mEPSCs, or the rise time and decay time of mEPSCs between the two groups of cells (sEPSCs: n = 13 endogenous and 6 grafted cells from 9and 4 mice, respectively; mEPSCs: n = 12 endogenous and 5 grafted cells from 6 and 3 mice, respectively). The data are expressed as mean ± SEM.

different micro-environments and generate distinctive cell types. Heterotopic grafting of NSCs from one niche to another effectively converted the developmental trajectories of neuronal progenitors and led to the generation of different neuronal subtypes with morpho-functional characteristics indistinguishable from endogenous neurons.

We carried out immunohistochemical, time-lapse imaging, and electrophysiological experiments to morphologically and functionally evaluate OE-derived NSCs. We first assessed the integration and proliferation of OE-derived NSCs in the SVZ niche. We did not observe any changes in cellular subtype or proliferation compared with endogenous cells. We then performed time-lapse imaging of GFP-labeled cells migrating along the RMS to the OB. Our results showed that the migration behavior of neuroblasts generated from OE NSCs is very similar to that of endogenous neuroblasts, including migration distance, migration vector, percentage of migratory phases, and migration speed. Following their migration through the RMS, these neuroblasts arrived in the OB where they matured and integrated the bulbar network at a similar pace and with similar morpho-functional characteristics as endogenous cells. We found that nearly all neurons derived from the OE-derived NSCs were located in the granule cell layer, which is in agreement with previous reports showing that the vast majority of adult-born neurons in the OB are granule cells (Malvaut and Saghatelyan, 2016; Winner et al., 2002). We further showed that mature neurons derived from OE NSCs have similar morphological profiles and receive the same excitatory inputs as endogenous cells in the OB. We also found no differences between these two groups of cells in terms of active and passive membrane properties, such as membrane resistance, resting membrane potential, capacitance, I_{Na+} activation threshold, or I_{Na+} peak amplitude. Although future studies using RNAseq are required to characterize the molecular phenotype of transplanted and endogenous cells, our results suggest that grafted and endogenous adult-born neurons are functionally identical.

Our results from the heterotopic grafting of OE-derived NSCs into adult mice not only highlighted the developmental potential and plasticity of OE-derived NSCs but also underscored the potential for using human OE-derived NSCs for studying human neurodevelopmental disorders

Table 1. The Intrinsic Passive and Active Membrane Properties of Endogenous Adult-Born Granule Cells and Neurons Derived from OE NSCs in the OB

	Endogenous	Grafted
Membrane resistance (GΩ)	1.06 ± 0.11	1.07 ± 0.08
Resting membrane potential (mV)	−62.77 ± 1.51	−60.14 ± 0.83
Capacitance (pF)	12.38 ± 0.68	12.71 ± 1.034
I_{Na}^+ threshold (mV)	31.54 ± 1.77	34.29 ± 2.97
I_{Na}^+ peak amplitude (pA)	−1,457.24 ± 175.66	−1,074.48 ± 169.92

No significant differences between the two populations of neurons were observed (n = 13 endogenous and 6 grafted cells from 9 and 4 mice, respectively).

and for developing autologous cell replacement therapies. In fact, the main reason for using OE-derived NSCs rather than other sources of NSCs is their accessibility and availability in the nasal cavity. Human NSCs have been isolated from the olfactory mucosa and have been successfully propagated *in vitro*. NSCs cultured from OE biopsies of schizophrenic patients have altered cell signaling pathways and dysregulated mitochondrial functions compared with NSCs from healthy controls (Matigian et al., 2010). However, it is important to note that non-neural skin fibroblasts and lymphoblasts from schizophrenia patients do not display such differences (Matigian et al., 2008, 2010), making olfactory NSCs a valuable cellular model for investigating the pathologies of brain disorders. It has also been shown that olfactory NSCs isolated from patients with Parkinson disease can generate dopaminergic cells *in vitro* similar to those derived from healthy controls. Once grafted into the unilaterally lesioned striatum of a Parkinson disease rat model, these NSCs can improve the behavioral asymmetry of these animals (Murrell et al., 2008). Our results also highlighted a higher propensity for integration of stem cells of neural lineage into the uninjured adult brain. Although several studies have shown that stem cells of other organs can integrate and functionally contribute to the regeneration of the injured/diseased nervous system (Carr et al., 2019; Sparling et al., 2015), the developmental potential and plasticity of grafted stem cells of different lineages in the uninjured brain remained unclear. The results of our detailed morpho-functional assessment of progenitors and neurons derived from OE NSCs after heterotopic grafting underline the potential and plasticity of OE-derived NSCs and add to the growing body of evidence suggesting that these cells may be used for modeling neurodevelopmental disorders and for developing cell replacement therapies.

EXPERIMENTAL PROCEDURES

Animals

Adult 2-month-old male C57BL/6 mice (Charles River) were used for the OE primary cultures and neurosphere grafting surgery. The experiments were performed in accordance with Canadian Guide for the Care and Use of Laboratory Animals guidelines. All the procedures involving animals were approved by the Université Laval animal protection committee. A maximum of four mice per cage were kept on a 12-h light/dark cycle at a constant temperature (22°C) with food and water *ad libitum*.

OE and Lamina Propria Primary Cultures and Neurosphere Induction

Olfactory mucosa biopsies from adult mice were collected according to a previously published protocol (Girard et al., 2011), with modifications. The primary culture of OE and lamina propria were prepared in parallel. In brief, olfactory mucosa was bilaterally isolated from anesthetized mice and was incubated in the dispase II solution (5 mg/mL) at 37°C for 45 min. After the incubation, OE sheets were carefully separated from lamina propria, the tissue was gently dissociated and cells were seeded in a T-25 flask precoated with poly-L-lysine (PLL) (5 μg/cm^2). To ascertain a clean separation of OE from the lamina propria, we performed immunohistochemical labeling for tissue-specific markers, such as CD90/Thy1 (Tome et al., 2009) and olfactory marker protein (OMP) (Liberia et al., 2019). Our data revealed that OE is well separated from the lamina propria (Figure S1). The dissociated cells were maintained in proliferation medium (DMEM/F12 supplemented with 10% fetal bovine serum [FBS] and 2% penicillin/streptomycin [P/S]), half of which was replaced every 2–3 days. When the primary culture reached confluency, the cells were trypsinized and replated in PLL-coated 6-well plates (0.85 μg/cm^2) for generating primary neurospheres. The cells were seeded at a density of 32,000/cm^2 and were cultured in induction medium (DMEM/F12 supplemented with 1% insulin-transferrin-selenium-ethanolamine [ITS-X], 50 ng/mL of epidermal growth factor [EGF], 50 ng/mL of fibroblast growth factor 2 [FGF2], and 2% P/S) for 3–4 weeks to reach the peak of neurosphere formation. For immunostaining experiments, floating OE-derived neurospheres were collected, dissociated in Accumax/Accutase (STEMCELL Technologies) and seeded on PLL-coated (15 μg/cm^2) coverslips.

The lamina propria was further cut into small pieces and subject to an additional incubation in the collagenase solution (0.25 mg/mL) at 37°C for 10 min. Following the enzymatic digestion, the tissues of lamina propria were collected, dissociated gently, and resuspended in proliferation medium (DMEM/F12 supplemented with 10% FBS and 2% P/S). The cell suspension was plated in PLL-coated (5 μg/cm^2) flasks. After reaching the confluence (at around 9–12 days), the cells were trypsinized, collected, and resuspended in the same induction medium used for OE neurospheres (DMEM/F12, 1% ITS-X, 50 ng/mL of EGF, 50 ng/mL of FGF2, and 2% P/S). The cells were seeded at a density of 32,000/cm^2 and were cultured in the same medium. Half of the induction medium was replenished every 2–3 days. After 1 week, the cells formed clusters and gave rise to floating spheres when they evolved into a 3D spherical structure capable of detaching. The

floating spheres continued to grow and were collected for further experiments. The peak of neurosphere formation from lamina propria-derived stem cells occurred at around 2 weeks after switching to the induction medium.

Viral Infection

Free-floating neurospheres were collected and were dissociated with Accumax at 37°C for 5 min. The cells were infected with the CMV-GFP (2.33×10^9 TU; Vector Core Facility, University of North Carolina [UNC]) or CMV-GFP (2.89×10^9 TU; SignaGen Laboratories) lentivirus. We used two different infection protocols and did not observe any difference in lentiviral transduction efficiency. In the first protocol, the lentiviral particles were added directly to the culture medium. A total of 100,000 dissociated cells with 1 μL of lentivirus were cultured in proliferation medium overnight before grafting. In the second protocol, we spin infected the cells with 0.1 μL of virus at 2,200 rpm for 60 min 1 day after plating the cells. The infected cells were then incubated at 37°C for a further 24 h. To collect cells for grafting, the medium was aspirated, and the cells were washed twice with PBS and then trypsinized at 37°C for 5 min. The detached cells were collected, washed twice with warm DMEM/F12, and resuspended in approximately 2 μL of DMEM/F12 for injection.

Stereotaxic Injection

The mice were anesthetized with 2%–3% isoflurane for the surgery, and the temperature was maintained at 37.5°C using an infrared blanket (Kent Scientific). For control mice, 100 nL of a GFP-encoding lentivirus (UNC Vector Core) was injected into two SVZ sites of both brain hemispheres of the adult mice (dorsal coordinates: anterior-posterior [AP], 0.7 mm; medial-lateral [ML], ±1.2 mm; dorsal-ventral [DV], –1.9 mm. ventral coordinates: AP, 0.9 mm; ML, ±1.0 mm; DV, –2.7 mm). For the grafting experiments, a minimum of 100,000 cells suspended in 2 μL of DMEM/F12 were injected (500 nL/site). After injection, the mice were kept for different periods of time (4, 8–9, 24–35 dpi) before being sacrificed. To ensure that the virally labeled cells after grafting were indeed OE-derived NSCs and not endogenous progenitors infected due to material exchange (Pearson et al., 2016; Santos-Ferreira et al., 2016; Singh et al., 2016), we infected neurospheres with EF1α-Cre-mCherry lentivirus (3.88×10^9 TU; SignaGen Laboratories) and grafted them into adult CAG-CAC-EGFP GFP-reporter mice (kindly provided by Dr. Kenneth Campbell, Cincinnati Children's Hospital Medical Center). We did not observe any GFP-expressing cells, indicating that the virally labeled cells were indeed derived from the graft and were not endogenous cells labeled due to material exchange.

Immunohistochemistry

The mice were anesthetized with pentobarbital (12 mg/mL, 0.1 mL per 10 g of body weight) and were perfused transcardially with 0.9% NaCl followed by 4% ice-cold paraformaldehyde (PFA). The brains were collected and were fixed in 4% PFA at 4°C overnight. Sagittal brain sections (40 μm) were obtained using a vibratome (Leica) from mice sacrificed at 4–9 dpi. Horizontal OB sections of (100 μm) were obtained from mice sacrificed at 24 or 60 dpi. The sections were incubated in blocking buffer (0.2% Triton X-100 and 4% milk diluted in PBS) at room temperature for 1 h and were then incubated with primary antibodies diluted in blocking buffer at 4°C overnight. The following primary antibodies were used: mouse anti-mCherry (1:1,000, no. 5411; Biovision), chicken (1:1,000, no. GFP-1020; Aves) and rabbit (1:1,000, no. A-11122; Thermo Fisher Scientific) anti-GFP, rabbit anti-Ki67 (1:1,000, no. ab15580; Abcam), mouse anti-Nestin (1:1,000, no. MAB353; Millipore), guinea pig anti-DCX (1:1,000, no. AB2253; Millipore), mouse anti-GFAP (1:1,000, no. MAB360; Millipore), goat anti-calretinin (1:1,000, no. AB1550; Millipore), rabbit anti-NeuN (1:500, no. 12943; Cell Signaling Technologies), goat anti-OMP (1:1,000, no. 544-10,001; WAKO), and rat anti-CD90/Thy1 (1:500, no. NBP1-28031; Novus). The anti-GFP antibodies were used to boost the signal in small dendritic spines. The sections were then washed in PBS three times before and after incubation with the corresponding secondary antibodies (1:1,000; Invitrogen) at room temperature for 3 h. DAPI was used to label nuclei. All the sections were mounted in fluorescence mounting medium (Dako) and were kept at 4°C before imaging using a confocal microscope (Olympus).

Time-Lapse Imaging

The mice were anesthetized with ketamine/xylazine (10 and 1 mg/mL, respectively, 0.1 mL per 10 g of body weight). The perfusion was performed transcardially with ice-cold oxygenated cutting solution containing (in mM) 210.3 sucrose, 3 KCl, 2 $CaCl_2$, 1.3 $MgCl_2$, 26 $NaHCO_3$, 1.25 NaH_2PO_4, and 20 glucose. Sagittal brain sections (250 μm) containing the SVZ-RMS-OB pathway were immediately transferred to oxygenated artificial cerebrospinal fluid (ACSF) maintained at 32°C and containing 125 mM NaCl, 3 mM KCl, 2 mM $CaCl_2$, 1.3 mM $MgCl_2$, 26 mM $NaHCO_3$, 1.25 mM NaH_2PO_4, and 20 mM glucose. During the time-lapse imaging, the acute sections were placed in a perfusion chamber maintained at 32°C with a flow of ACSF (1–2 mL/min). z stack images were taken for 60 min with an acquisition interval of 15 s. Videos were analyzed using Imaris (Bitplane) software and the values for vector displacement and total length were extracted directly from Imaris software. The percentage of migratory phases was assessed based on the speed profile of each individual cell visualized using Origin software. We took into account only migratory periods intercepted by stationary phases, and calculated the speed of migration only during the migratory phases.

Patch-Clamp Recordings

At 28–35 dpi, deeply anesthetized mice were transcardially perfused with modified oxygenated ACSF containing sucrose, as described above. Horizontal sections of the OBs (250 μm) were obtained and were superfused with oxygenated ACSF supplemented with NaCl, as described above. Recordings were performed using a Multiclamp 700B amplifier (Molecular Devices) and a Digidata 1440A digitizer (Molecular Devices). Glass patch electrodes (7–9 MΩ) were filled with a solution containing 122.5 mM K-gluconate, 10 mM KCl, 10 mM HEPES, 0.2 mM EGTA, 10 mM glucose, 2 mM MgATP, and 0.3 mM NaGTP, as well as 5 μM Alexa Fluor 594 (Life Technology). The Alexa Fluor 594 was added to the patch solution to ensure that the recordings were indeed from virally labeled neurons. (−)-Bicuculline methochloride or methiodide (BMI) (50 μM; Abcam) was used as

a GABAA receptor antagonist to isolate sEPSCs. Tetrodotoxin citrate (1 μM; Tocris Bioscience) was added in the presence of BMI to block voltage-dependent sodium channels in order to isolate mEPSCs. Cells were held at the holding potential of −60 mV. Voltage pulses of 200 ms from −100 to 20 mV in 10-mV increments were applied. Synaptic responses were continuously recorded for 3 min and were analyzed using the MiniAnalysis program (Synaptosoft).

SUPPLEMENTAL INFORMATION

Supplemental Information can be found online at https://doi.org/10.1016/j.stemcr.2020.03.008.

AUTHOR CONTRIBUTIONS

Q.L. performed most of the experiments and analyzed the data. T.S. performed electrophysiological characterization of endogenous and grafted cells. C.B. performed time-lapse imaging of endogenous neuroblasts and immunohistochemical characterization of cells in vitro. Y.d.K. and A.S. obtained fundings. A.S. designed and supervised the study. Q.L. and A.S. wrote the manuscript, taking into consideration the comments of the other authors.

ACKNOWLEDGMENTS

We thank Dr. Marina Snapyan for establishment and help with olfactory epithelium cultures. This work was supported by the Canadian Institutes of Health Research (CIHR) grant PJT-159733 to A.S. and endowed chair funds to Y.d.K. The authors declare no conflict of interests.

Received: July 19, 2019
Revised: March 5, 2020
Accepted: March 6, 2020
Published: April 2, 2020

REFERENCES

Abdel-Rahman, M., Galhom, R.A., El-Din, W.A.N., Ali, M.H.M., and Abdel-Hamid, A.E.-D.S. (2018). Therapeutic efficacy of olfactory stem cells in rotenone induced Parkinsonism in adult male albino rats. Biomed. Pharmacother. *103*, 1178–1186.

Alonso, M., Lepousez, G., Wagner, S., Bardy, C., Gabellec, M.-M., Torquet, N., and Lledo, P.-M. (2012). Activation of adult-born neurons facilitates learning and memory. Nat. Neurosci. *15*, 897.

Alvarez-Buylla, A., and Garcıa-Verdugo, J.M. (2002). Neurogenesis in adult subventricular zone. J. Neurosci. *22*, 629–634.

Andrews, P.J., Poirrier, A.-L., Lund, V.J., and Choi, D. (2016). Safety of human olfactory mucosal biopsy for the purpose of olfactory ensheathing cell harvest and nerve repair: a prospective controlled study in patients undergoing endoscopic sinus surgery. Rhinology *54*, 183–191.

Ayala-Grosso, C.A., Pieruzzini, R., Diaz-Solano, D., Wittig, O., Abrante, L., Vargas, L., and Cardier, J. (2015). Amyloid-abeta peptide in olfactory mucosa and mesenchymal stromal cells of mild cognitive impairment and Alzheimer's disease patients. Brain Pathol. *25*, 136–145.

Brann, J.H., Ellis, D.P., Ku, B.S., Spinazzi, E.F., and Firestein, S. (2015). Injury in aged animals robustly activates quiescent olfactory neural stem cells. Front. Neurosci. *9*, 367.

Breton-Provencher, V., Lemasson, M., Peralta, M.R., and Saghatelyan, A. (2009). Interneurons produced in adulthood are required for the normal functioning of the olfactory bulb network and for the execution of selected olfactory behaviors. J. Neurosci. *29*, 15245–15257.

Carleton, A., Petreanu, L.T., Lansford, R., Alvarez-Buylla, A., and Lledo, P.-M. (2003). Becoming a new neuron in the adult olfactory bulb. Nat. Neurosci. *6*, 507.

Carr, M.J., Toma, J.S., Johnston, A.P.W., Steadman, P.E., Yuzwa, S.A., Mahmud, N., Frankland, P.W., Kaplan, D.R., and Miller, F.D. (2019). Mesenchymal precursor cells in adult nerves contribute to mammalian tissue repair and regeneration. Cell Stem Cell *24*, 240–256.e9.

Cook, A.L., Vitale, A.M., Ravishankar, S., Matigian, N., Sutherland, G.T., Shan, J., Sutharsan, R., Perry, C., Silburn, P.A., and Mellick, G.D. (2011). NRF2 activation restores disease related metabolic deficiencies in olfactory neurosphere-derived cells from patients with sporadic Parkinson's disease. PLoS One *6*, e21907.

Fan, J.-R., Lee, H.-T., Lee, W., Lin, C.-H., Hsu, C.Y., Hsieh, C.-H., and Shyu, W.-C. (2018). Potential role of CBX7 in regulating pluripotency of adult human pluripotent-like olfactory stem cells in stroke model. Cell Death Dis. *9*, 502.

Feron, F., Gepner, B., Lacassagne, E., Stephan, D., Mesnage, B., Blanchard, M.P., Boulanger, N., Tardif, C., Deveze, A., and Rousseau, S. (2016). Olfactory stem cells reveal MOCOS as a new player in autism spectrum disorders. Mol. Psychiatry *21*, 1215.

Gengatharan, A., Bammann, R.R., and Saghatelyan, A. (2016). The role of astrocytes in the generation, migration, and integration of new neurons in the adult olfactory bulb. Front. Neurosci. *10*, 149.

Girard, S.D., Devéze, A., Nivet, E., Gepner, B., Roman, F.S., and Féron, F. (2011). Isolating nasal olfactory stem cells from rodents or humans. J. Vis. Exp. https://doi.org/10.3791/2762.

Grelat, A., Benoit, L., Wagner, S., Moigneu, C., Lledo, P.-M., and Alonso, M. (2018). Adult-born neurons boost odor–reward association. Proc. Natl. Acad. Sci. U S A *115*, 2514–2519.

Hardy, D., Malvaut, S., Breton-Provencher, V., and Saghatelyan, A. (2018). The role of calretinin-expressing granule cells in olfactory bulb functions and odor behavior. Sci. Rep. *8*, 9385.

Lavoie, J., Sawa, A., and Ishizuka, K. (2017). Application of olfactory tissue and its neural progenitors to schizophrenia and psychiatric research. Curr. Opin. Psychiatry *30*, 176.

Liberia, T., Martin-Lopez, E., Meller, S.J., and Greer, C.A. (2019). Sequential maturation of olfactory sensory neurons in the mature olfactory epithelium. eNeuro *6*. https://doi.org/10.1523/ENEURO.0266-19.2019.

Lledo, P.-M., and Saghatelyan, A. (2005). Integrating new neurons into the adult olfactory bulb: joining the network, life–death decisions, and the effects of sensory experience. Trends Neurosci. *28*, 248–254.

Mackay-Sim, A., and Kittel, P. (1991). Cell dynamics in the adult mouse olfactory epithelium: a quantitative autoradiographic study. J. Neurosci. *11*, 979–984.

Malvaut, S., Gribaudo, S., Hardy, D., David, L.S., Daroles, L., Labrecque, S., Lebel-Cormier, M.-A., Chaker, Z., Coté, D., and De Koninck, P. (2017). CaMKIIα expression defines two functionally distinct populations of granule cells involved in different types of odor behavior. Curr. Biol. *27*, 3315–3329.e6.

Malvaut, S., and Saghatelyan, A. (2016). The role of adult-born neurons in the constantly changing olfactory bulb network. Neural Plast. *2016*, 1614329.

Matigian, N.A., McCurdy, R.D., Feron, F., Perry, C., Smith, H., Filippich, C., McLean, D., McGrath, J., Mackay-Sim, A., and Mowry, B. (2008). Fibroblast and lymphoblast gene expression profiles in schizophrenia: are non-neural cells informative? PLoS One *3*, e2412.

Matigian, N., Abrahamsen, G., Sutharsan, R., Cook, A.L., Vitale, A.M., Nouwens, A., Bellette, B., An, J., Anderson, M., and Beckhouse, A.G. (2010). Disease-specific, neurosphere-derived cells as models for brain disorders. Dis. Model. Mech. *3*, 785–798.

Murrell, W., Féron, F., Wetzig, A., Cameron, N., Splatt, K., Bellette, B., Bianco, J., Perry, C., Lee, G., and Mackay-Sim, A. (2005). Multipotent stem cells from adult olfactory mucosa. Dev. Dyn. *233*, 496–515.

Murrell, W., Wetzig, A., Donnellan, M., Féron, F., Burne, T., Meedeniya, A., Kesby, J., Bianco, J., Perry, C., and Silburn, P. (2008). Olfactory mucosa is a potential source for autologous stem cell therapy for Parkinson's disease. Stem Cells *26*, 2183–2192.

Nagayama, S., Homma, R., and Imamura, F. (2014). Neuronal organization of olfactory bulb circuits. Front. Neural Circuits *8*, 98.

Nguyen, L.S., Lepleux, M., Makhlouf, M., Martin, C., Fregeac, J., Siquier-Pernet, K., Philippe, A., Feron, F., Gepner, B., and Rougeulle, C. (2016). Profiling olfactory stem cells from living patients identifies miRNAs relevant for autism pathophysiology. Mol. Autism *7*, 1.

Pearson, R.A., Gonzalez-Cordero, A., West, E.L., Ribeiro, J.R., Aghaizu, N., Goh, D., Sampson, R.D., Georgiadis, A., Waldron, P.V., and Duran, Y. (2016). Donor and host photoreceptors engage in material transfer following transplantation of post-mitotic photoreceptor precursors. Nat. Commun. *7*, 13029.

Santos-Ferreira, T., Llonch, S., Borsch, O., Postel, K., Haas, J., and Ader, M. (2016). Retinal transplantation of photoreceptors results in donor–host cytoplasmic exchange. Nat. Commun. *7*, 13028.

Schroeder, E., Gao, Y., Lei, Z., Roisen, F., and El-Mallakh, R.S. (2016). The gene BRAF is underexpressed in bipolar subject olfactory neuroepithelial progenitor cells undergoing apoptosis. Psychiatry Res. *236*, 130–135.

Seidenfaden, R., Desoeuvre, A., Bosio, A., Virard, I., and Cremer, H. (2006). Glial conversion of SVZ-derived committed neuronal precursors after ectopic grafting into the adult brain. Mol. Cell. Neurosci. *32*, 187–198.

Shihabuddin, L.S., Horner, P.J., Ray, J., and Gage, F.H. (2000). Adult spinal cord stem cells generate neurons after transplantation in the adult dentate gyrus. J. Neurosci. *20*, 8727–8735.

Singh, M.S., Balmer, J., Barnard, A.R., Aslam, S.A., Moralli, D., Green, C.M., Barnea-Cramer, A., Duncan, I., and MacLaren, R.E. (2016). Transplanted photoreceptor precursors transfer proteins to host photoreceptors by a mechanism of cytoplasmic fusion. Nat. Commun. *7*, 13537.

Sparling, J.S., Bretzner, F., Biernaskie, J., Assinck, P., Jiang, Y., Arisato, H., Plunet, W.T., Borisoff, J., Liu, J., Miller, F.D., et al. (2015). Schwann cells generated from neonatal skin-derived precursors or neonatal peripheral nerve improve functional recovery after acute transplantation into the partially injured cervical spinal cord of the rat. J. Neurosci. *35*, 6714–6730.

Suhonen, J.O., Peterson, D.A., Ray, J., and Gage, F.H. (1996). Differentiation of adult hippocampus-derived progenitors into olfactory neurons in vivo. Nature *383*, 624.

Tome, M., Lindsay, S.L., Riddell, J.S., and Barnett, S.C. (2009). Identification of nonepithelial multipotent cells in the embryonic olfactory mucosa. Stem Cells *27*, 2196–2208.

Whitman, M.C., and Greer, C.A. (2007). Synaptic integration of adult-generated olfactory bulb granule cells: basal axodendritic centrifugal input precedes apical dendrodendritic local circuits. J. Neurosci. *27*, 9951–9961.

Winner, B., Cooper-Kuhn, C.M., Aigner, R., Winkler, J., and Kuhn, H.G. (2002). Long-term survival and cell death of newly generated neurons in the adult rat olfactory bulb. Eur. J. Neurosci. *16*, 1681–1689.

Xu, Y.-P., Shan, X.-D., Liu, Y.-Y., Pu, Y., Wang, C.-Y., Tao, Q.-L., Deng, Y., Cheng, Y., and Fan, J.-P. (2016). Olfactory epithelium neural stem cell implantation restores noise-induced hearing loss in rats. Neurosci. Lett. *616*, 19–25.